Electric field tunable superconductivity with competing orders in twisted bilayer graphene near magic-angle

Ranit Dutta,[†,‡] Ayan Ghosh,[†,‡] Shinjan Mandal,[‡] Kenji Watanabe,[¶] Takashi Taniguchi,[§] H. R. Krishnamurthy,[‡] Sumilan Banerjee,[‡] Manish Jain,[‡] and Anindya Das[*,‡]

†*These authors contributed equally to this work*

‡*Department of Physics, Indian Institute of Science, Bangalore 560012, India*

¶*Research Center for Functional Materials, National Institute for Materials Science, 1-1 Namiki, Tsukuba 305-0044, Japan*

§*International Center for Material Nanoarchitectonics, National Institute for Materials Science, 1-1 Namiki, Tsukuba 305-0044, Japan*

E-mail: anindya@iisc.ac.in

Abstract

Superconductivity (SC) in twisted bilayer graphene (tBLG) has been explored by varying carrier concentrations, twist angles, and screening strength, with the aim of uncovering its origin and possible connections to strong electronic correlations in narrow bands and various resulting broken symmetries. However, the link between the tBLG band structure and the onset of SC and other orders largely remains unclear. In this study,

we address this crucial gap by examining in-situ band structure tuning of a near magic-angle ($\theta \approx 0.95°$) tBLG device with displacement field (D) and reveal competition between SC and other broken symmetries. At zero D, the device exhibits superconducting signatures without the resistance peak at half-filling, a characteristic signature with a strong electronic correlation. As D increases, the SC is suppressed, accompanied by the appearance of a resistance peak at half-filling. Hall density measurements reveal that at zero D, SC arises around the van Hove singularity (vHs) from an isospin or spin-valley unpolarized band. At higher D, the suppression of SC coincides with broken isospin symmetry near half-filling with lifted degeneracy ($g_d \sim 2$). Additionally, as the SC phase becomes weaker with D, vHs shifts to higher fillings, highlighting the modification of the underlying band structure with the applied electric field. These findings, with recent theoretical study on SC in tBLG, highlight the competition, rather being connected concomitantly, between SC and other orders promoted by broken symmetries.

KEYWORDS: Twistronics, superconductivity, near magic-angle twisted bilayer graphene, displacement field, Hall filling, isospin broken symmetry, van Hove singularity

A relative twist angle between two or more van der Waals layers,[1–11] leading to the formation of moiré superlattice, has opened up a completely new field of condensed matter research known as 'twistronics'. Observations of interaction-driven emergent phenomena like superconductivity (SC),[1,2,6,8–21] correlated Mott insulators,[2,3] orbital ferromagnetism,[22] anomalous Hall[23] and quantized anomalous Hall effect,[24] nematicity,[13] Chern insulators,[25–29] strange metal,[30] giant thermopower[14] and breakdown of semi-classical description of Mott's formula[14,31,32] are ubiquitous in this area. Among the family of twisted heterostructures, magic-angle twisted bilayer graphene (MAtBLG)[1–3,12,13,17,19,26,27,30,33–36] with a twist angle of $\theta_M \simeq 1.05^\circ - 1.1^\circ$ between two sheets of graphene monolayer is being extensively studied for hosting flat bands[37] and having a rich phase diagram with such strongly correlated phases. Inter-layer hybridization between the rotated layers facilitates the formation of these isolated flat bands which causes the effective electronic kinetic energy to become much smaller than the effective coulomb interactions[3] leading to the realization of such correlated phases. The appearance of correlated insulators (CI)[2,3] at integer moiré filling ν and a superconducting dome when the CIs are doped away from the integer filling[1,2] shows a strong resemblance to the behavior of high-T_c (> 100 K) cuprate superconductors .[38]

Recent studies have, however, raised questions as to whether and to what extent superconductivity in tBLG is intimately connected with correlation effects.[16–18] In these reports, superconductivity has been observed even in the absence of correlated insulator states by varying the dielectric thickness to control the coulomb screening,[17] and even at angles detuned away from θ_M, with the SC phase sometimes taking over the whole of the phase space without any signature of correlated states.[16–18] The decoupling of superconductivity and correlated insulator behavior in the presence of screened coulomb interactions[19] or the increased bandwidth of the flat bands (angles away from $\theta_M \pm 0.05^o$) indicate that these two phenomena may not be always intimately connected, and may even be competing[17,18] and electron-phonon mechanism may be playing a significant role in the origin of superconductivity in tBLG.[17,39–41] Thus, unlike other graphene-based systems such as Bernal bilayer graphene (BBG),[42–44] rhombohedral trilayer graphene (RTG),[45] ABC-trilayer graphene/aligned with hBN,[46] alternatingly twisted trilayer,[8,9] and multilayer graphene,[10,11] where superconductivity consistently emerges close to other symmetry-broken phases, it remains unclear whether superconductivity and other symmetry-broken phases are fundamentally linked in twisted bilayer graphene (tBLG).

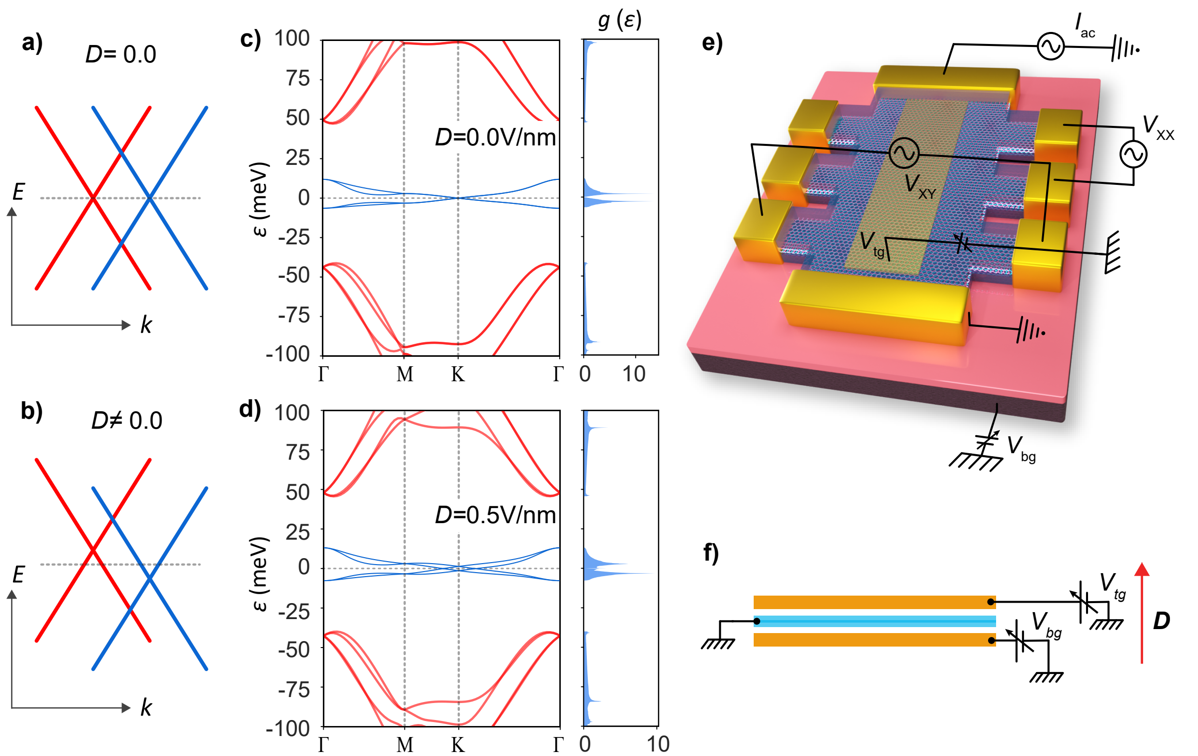

Figure. 1: Band structure and device schematic. Schematic presentation of band crossing of top and bottom layer graphene at **a)** zero D, and **b)** finite D, . The calculated band structures using a tight-binding model on relaxed structures of twist angle, $\theta \sim 0.95°$ tBLG for **c)** $D = 0$, and **d)** $D = 0.5$ V/nm (For the theoretical calculation of D see Methods and Supplementary Information SI-15 (II)). **e)** Device set-up for measuring R_{xx} and R_{xy}. Using the combination of a metal top gate (V_{tg}) and a global SiO_2/Si back gate (V_{bg}), the carrier density, n, and the perpendicular displacement field, D, were controlled independently. **f)** The schematic for the positive displacement field when V_{bg} is positive but V_{tg} is negative. All the measurements are done with constant current bias and using a standard low-frequency lock-in technique at frequency $f = 13$ Hz in a cryo-free dilution refrigerator.

To answer these questions, one needs to investigate specific features of tBLG, other than electron-electron and electron-phonon interaction, *e.g.*, band structure details such as van Hove singularity (vHs) that can crucially influence superconductivity. However, the exploration of how the appearance of superconductivity is connected to the features of such band structure details in tBLG is missing in the literature. Here, we address this issue through the *in situ* tuning of the band structure by a displacement field that continuously tunes a vHs further away from half-filling and thus induces other symmetry-breaking orders, presumably competing with SC. As shown schematically in Figure. 1a-d, applying a perpendicular electric field can tune the band structure of a tBLG with a twist angle slightly away from the magic angle, and can give insights into the intimate connection between the band structure and SC. Thus, we present a comprehensive study on tuning the SC phase of a near magic-angle tBLG ($\sim 0.95°$) device as a function of a perpendicular electric field (displacement field, D). At zero displacement field ($D = 0.00$ V/nm), the device shows resistance peaks at the Dirac point (CNP) and full band filling ($\nu = \pm 4$) also known as superlattice gaps, but without any signature of resistance peaks at half-filling ($\nu \sim \pm 2$). Most interestingly, the device shows the signature of SC with resistance dropping to almost zero with decreasing temperature away from half-filling ($\nu \sim +2.7$). Typical behaviors such as a superconducting dome with temperature (T), non-linear current-voltage ($I - V$) characteristics, and suppression of the superconducting phase with a magnetic field ($B_{\perp}$) establish the robustness of the SC phase of the device at $D = 0.00$ V/nm. With increasing D, the SC phase is suppressed with the appearance of the resistance peak at the half-filling ($\nu \sim +2$). The tuning of the SC is further quantified from the D dependent critical temperature, T_c, critical current, I_c, and critical magnetic field, B_c, (both parallel and perpendicular). To understand the role of the band structure, we study the Hall density (Hall filling/Normalized Hall density, ν_H) as a function of the filling (ν) at different D, which reveals the following: (i) at $D = 0.00$ V/nm, the SC arises precisely around the van Hove singularity (vHs) from an isospin-unpolarized band with degeneracy, $g_d = 4$, (ii) at higher D magnitudes, the suppression of SC is concomitant with the broken isospin symmetry near half-filling, with lifted degeneracy of $g_d \sim 2$.

Results and Discussion

Device set-up and characterization

For our study, we have fabricated a dual-gated hBN encapsulated twisted bilayer graphene device using the modified 'cut and stack' technique from an exfoliated single monolayer graphene sheet on a SiO_2/Si substrate.[47] Fabrication details are mentioned in the Supplementary Information SI- 1. A metal layer above the top hBN acts as the top gate of the device, whereas the silicon (Si) layer acts as the global back gate. The dual-gated device structure helps to tune the total number density, n, and the perpendicular displacement field, D, independently [4–9] in our tBLG device, as shown schematically in Figure. 1f (see SI- 2 for details). Figure. 1e shows the device schematic together with the measurement scheme to measure longitudinal (R_{xx}) and transverse (R_{xy}) resistance in a standard Hall-bar geometry set-up. Figure. 2a shows the longitudinal resistance, R_{xx}, versus the filling factor, ν, with increasing temperature from the base temperature of $T = 20$ mK up to 25 K at $D = 0.00$ V/nm. The carrier density, n, measured relative to the charge neutrality point (CNP) is converted to moiré filling factor, $\nu = \frac{4n}{n_s}$, where n_s is the requisite carrier density to fill/empty the low energy flat bands (*i.e.*, 4 electron/holes per moiré superlattice

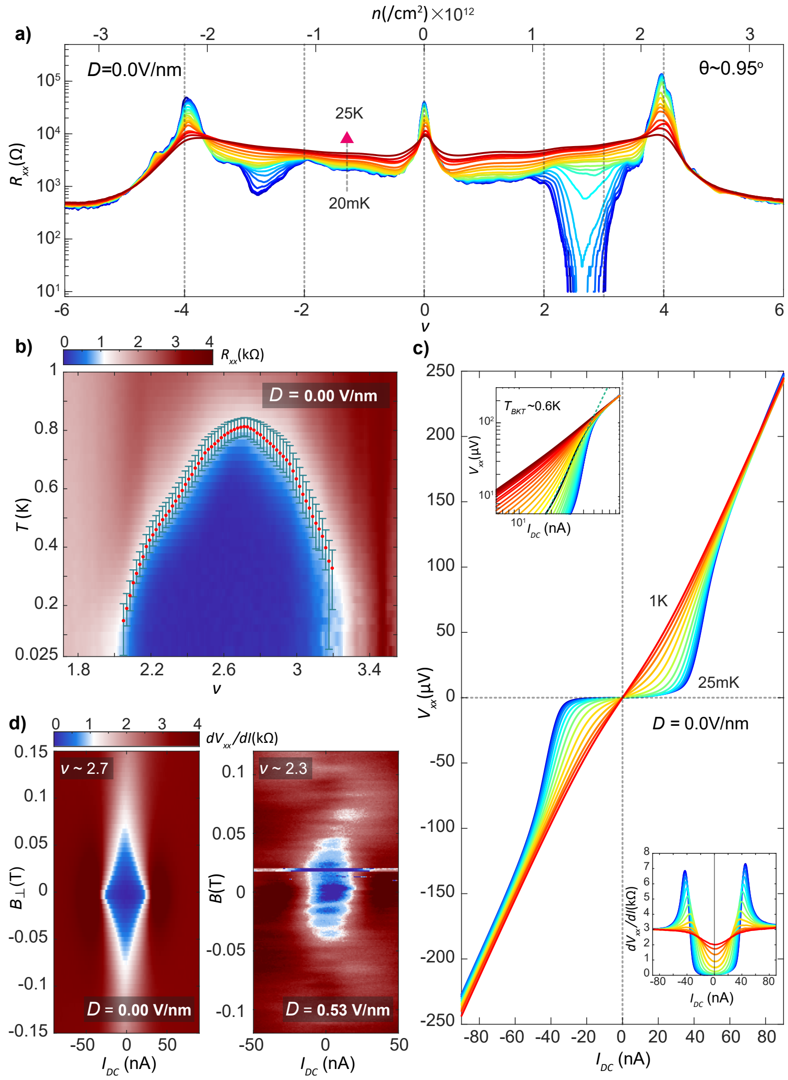

Figure. 2: Robust superconductivity at zero D. a) Measured R_{xx} versus carrier filling, ν, from $T = 20$ mK up to 25 K at $D = 0$ V/nm. The resistance peaks at the Dirac point, and full band filling ($\nu = +4, -4$) are seen without any signature of resistance peaks at other integer fillings. The R_{xx} value approaches close to zero on the electron side at $T = 20$ mK between $\nu \sim 2-3$ marking the superconducting region. **b)** 2−d colormap of R_{xx} as a function of ν and T showing the superconductivity dome around optimal doping ($\nu_c \sim 2.6 - 2.7$). The red dots are the critical temperatures, T_c, corresponding to the 50% value of normal state resistance, R_n. The error bars refer to the corresponding temperatures, T, at which R_{xx} drops to 60% and 40% of R_n. **c)** $I - V$ characteristics of SC region at $\nu \approx +2.7$ with variation of T from 25 mK to 1 K. The lower inset shows the dV_{xx}/dI versus I_{DC}. In the upper inset, $V_{xx} \propto I^3$ behavior is seen suggesting a typical 2D superconductor with a Berezinskii-Kosterlitz-Thouless transition at $T_{BKT} \sim 600$ mK. **d)** dV_{xx}/dI versus I_{DC} and $B_\perp$ for $(\nu, D) = +2.7, 0.0$ V/nm (left panel) and $+2.3, 0.5$ V/nm (right panel). The Fraunhofer-like oscillations can be seen when the SC is suppressed at higher D near the edge of the SC dome.

unit cell).[1,2] High insulating resistance peaks at moiré integer filling, $\nu = \pm 4$, on either side of the CNP indicates the presence of a single-particle band gap above and below the low energy flat bands. The twist angle from the carrier densities for $\nu = \pm 4$ corresponds to $\theta \approx 0.95° \pm 0.02°$ for our device, which is around 13% smaller than the magic angle $\theta_M \approx 1.1^0$. Unlike other tBLG devices closer to the magic-angle,[1–3,12,17,18] we do not observe any resistance peaks corresponding to the correlated insulators at half-filling, $\nu = \pm 2$, or at other integer fillings.[2] In SI-6, we discuss various origins for the absence of resistance peaks at half-filling. All the measurements are done using the standard lock-in technique at $f \sim 13$ Hz in a cryo-free dilution fridge for several thermal cycles.

Superconductivity at zero D

As seen in Figure. 2a, we see a clear signature of superconductivity on the electron side with the R_{xx} value going down to almost zero between $\nu = +2.2$ and $\nu = +3$ at the base temperature of $T = 20$ mK. Though the signature of resistance decrement with lowering of the temperature on the hole side between $\nu = -2.2$ and $\nu = -3$ can be seen in Figure. 2a, in this region the R_{xx} value remains finite at the lowest measured temperature (~ 20 mK). From here on, we will only focus on the superconducting region on the electron side ($+2 < \nu < +3$). Figure. 2b shows $R_{xx}(\nu, T)$ in the 2−d colormap. A superconducting dome around $\nu_c \sim 2.6 - 2.7$ (optimal doping) is visible clearly. The temperature dependence of V_{xx} versus I_{DC} traces are shown in Figure. 2c, which is obtained by integrating dV_{xx}/dI as a function of I_{DC} as shown in the lower inset of Figure. 2c. The traces in Figure. 2c show the classic evolution of 2D superconductors from step-like transitions at low temperature to ohmic dependence around 1 K. The upper inset in Figure. 2c shows the BKT (Berezinskii-Kosterlitz-Thouless) transition, where the evolution of the $V_{xx} \sim I_{DC}^{\alpha}$ power law near the critical bias current gives the BKT transition temperature, $T_{BKT} \sim 0.6$ K corresponding to $V_{xx} \sim I_{DC}^{3}$. Figure. 2b and 2c establish the robustness of the superconductivity in our device at $D = 0.00$ V/nm. Further, the superconductivity is killed by applying a perpendicular magnetic field ($B_{c\perp} \approx 60 - 70$ mT) as shown in Figure. 2d-left panel for the optimal doping position ($\nu \sim 2.7$). In SI-4 and SI-5 sections, we compare the response of the device with $B_{\perp}$ at the optimal doping and near the edge of the superconductivity dome for $D = 0.00$ V/nm and finite D. The Fraunhofer-like oscillation pattern[1,2,6,8,12,14,16] is not seen at $D = 0.00$ V/nm, and it only emerges (SI-Fig. 6,7) near the edge of the superconductivity dome at larger D as shown in Figure. 2d-right panel for $\nu \sim 2.3$. The absence of the Fraunhofer pattern at $D = 0.00$ V/nm suggests the existence of a more homogeneous SC phase[48] in our device. These observations critically establish the occurrence of a robust 2D superconductivity[1,2,8,9,16–18] seen here in the near MAtBLG at zero D. At larger D when the superconductivity gets suppressed, which will be discussed in the next section, the pockets of superconducting and non-superconducting (normal region) puddles are formed near the edge of the superconductivity dome resulting in the network of Josephson junctions, which allows the Fraunhofer pattern to emerge. From the quasi-periodic oscillations of the Fraunhofer pattern shown in Figure. 2d-right panel and SI-Fig. 7, the effective area of the superconducting puddles found to be ~ 0.2 μm^2, in comparison to our device channel area between the R_{xx} measurement probes ~ 10 μm^2. The estimated puddle size is in qualitative agreement with earlier studies.[1,8,16,17]

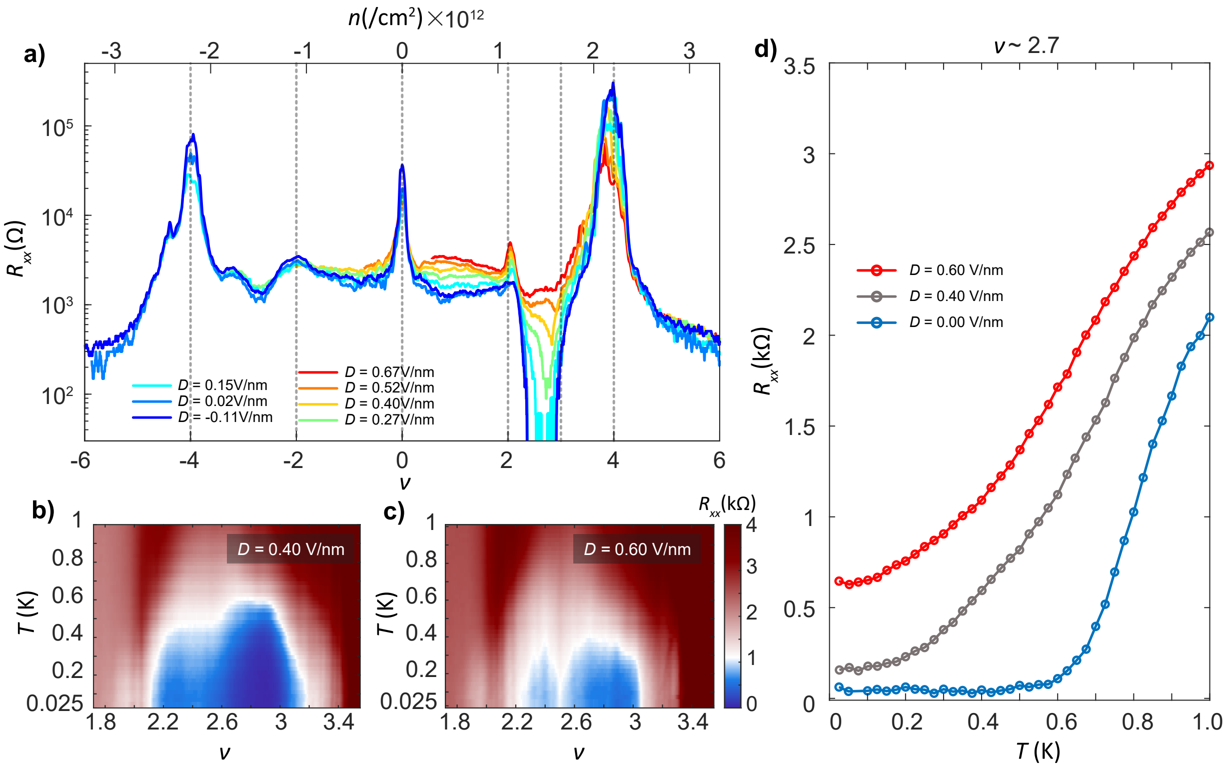

Figure. 3: Tunability of superconductivity with D. a) R_{xx} versus ν at the base temperature for different D. The SC weakens with increasing D, and a resistance peak emerges at $\nu \sim 2$ with a background resistance increment around $\nu \sim 1$. **b)** and **c)** represent the superconducting domes of $R_{xx}(\nu, T)$ for $D = 0.40$ V/nm and 0.60 V/nm, respectively. The superconducting domes' width and height decrease with increasing D compared to the zero D case in Figure. 2b. **d)** Plots of R_{xx} vs. T for different D fields at $\nu \sim 2.7$.

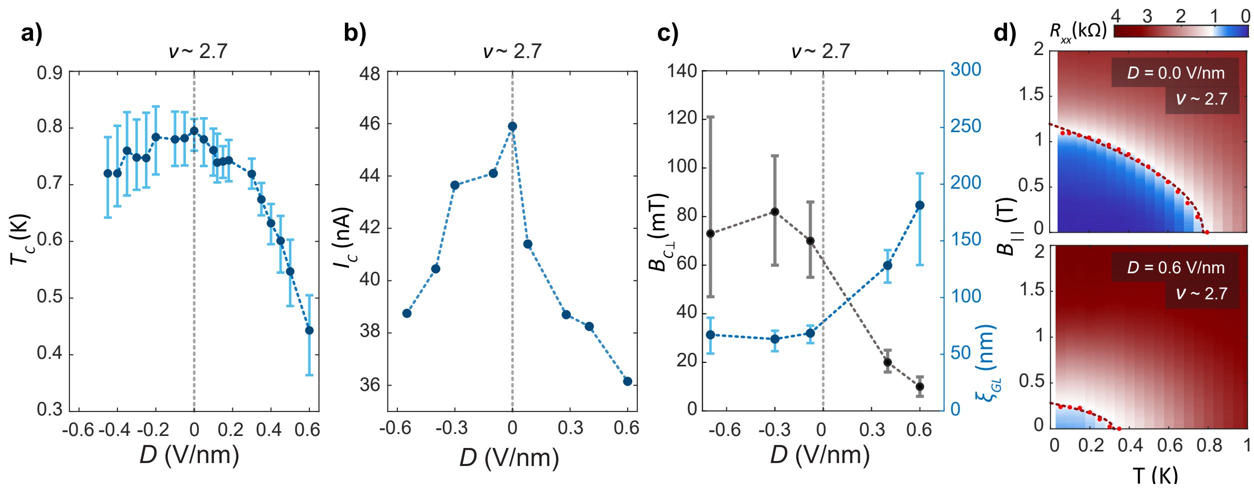

Figure. 4: Superconductivity metrics with D. **a)** Variation of T_c with D at $\nu \sim +2.7$. The values of T_c were approximated as the temperatures at which R_{xx} drops to 50% of normal state resistance, R_n, for the respective D fields. The error bars represent the temperatures corresponding to 60% and 40% of R_n. **b)** Variation of I_c with D at $\nu \sim +2.7$. **c)** Variation of $B_{c\perp}$ (left axis) and corresponding Ginzburg-Landau coherence length, ξ_{GL} (right axis), with D at $\nu \sim +2.7$. The error bars for $B_{c\perp}$ represent the required magnetic field, $B_\perp$, to cross 60% and 40% thresholds of R_n. **d)** R_{xx} versus $B_\parallel$ and T for zero D (top panel) and 0.60 V/nm (bottom panel). The temperature dependence of $B_{c\parallel}$ (red dots) is fitted (dashed black line) to extract the critical parallel magnetic field at zero temperature, $B^0_{c\parallel} \sim 1.2$ T and 0.3 T for $D = 0.00$ V/nm and 0.60 V/nm, respectively, which matches well with the Pauli limit calculated from $B_P = 1.76 k_B T^0_c \sqrt{2}/g\mu_B$, where T^0_c is the zero magnetic field critical temperature, g is the Landé g-factor, and μ_B is Bohr magneton.

Tuning the strength of the SC phase with D

In this section, we discuss our main results on tuning the SC with D. Figure. 3a shows the variation of R_{xx} with ν at the base temperature for several D. The corresponding 2−d colormap of R_{xx} with ν and D is shown in SI-Fig. 2a. As shown in Figure. 3a, with increasing positive D, the resistance peak values at the CNP and full band filling ($\nu = \pm 4$) slightly decrease while the most dramatic effect with D can be seen on the electron-doped side, particularly between $\nu \sim 1 - 3$. The superconducting region's width around $\nu \sim +2.7$ gradually shrinks as the D value crosses $\geq +0.25$ V/nm. As SC weakens with D, a resistance peak emerges at $\nu \sim +2$ together with an increase in the background resistance value around $\nu \sim +1$. This could be an indication of the onset of correlation physics, which is discussed in the next section while presenting the Hall density measurements. The concomitance between the SC suppression and resistance peak appearance with increasing D suggest that the two phases compete rather than being intimately connected. However, at zero D, it might be possible that the proximity of the strong SC phase suppresses the resistance peak. To distinguish, in SI-Fig. 8, the R_{xx} with ν shown at $B_\perp = 0$ and ~ 100 mT. At $B_\perp \sim 100$ mT, the SC is completely killed, but the resistance peak can hardly be seen at the half-filling. This indicates that at $D \approx 0$ V/nm, the signature of correlation at the half-filling is weaker in our device. Note that the strength of SC also decreases with negative D, but the effect remains weaker compared to the positive D as discussed in SI- 3 (I) (see SI-Fig. 2b). The superconducting region being tuned by D has already been reported in other systems like alternatingly twisted magic-angle trilayer graphene, [8,9] quadra layer and pentalayer [10,11] graphene, but not so far seen in tBLG. Ref[12] on MAtBLG reports an appearance of a resistive peak at half filling on the hole side ($\nu = -2$) with increasing D (negative to positive). The apparent asymmetric behavior in the SC phase with D (near $|\nu| \sim 2$) is attributed to the structural inhomogeneity in the device but there are no indications of the nature of modification of the strength of the superconducting phase with D in the study.[12] Here, we have tried to uncover the nature of the tuning of the strength of the SC phase with D in a near magic-angle twisted bilayer graphene.

The tunability of the SC phase in our near magic-angle tBLG can be further seen in the superconducting dome, as shown in Figure. 3b and 3c. It can be seen that compared to Figure. 2b at $D = 0.00$ V/nm, at $D = 0.40$ V/nm and 0.60 V/nm in Figure. 3b,c both the width (in ν) of the SC region and T_c are reduced significantly. Figure. 3d shows R_{xx} versus T at the optimal doping ($\nu \sim +2.7$) for several D, emphasizing the tunability of SC with D. In Figure. 4, we have summarized the tunability of several SC metrics with D. The variation of T_c, I_c, and $B_{c\perp}$ with D are shown in Figure.s 4a, 4b, 4c respectively. Raw data related to these plots are shown in SI- 7 and SI- 8 (SI-Fig.s 9-13); which also describes the method (R_{xx} value to one-half of its normal state value[2,6,8]) used to extract T_c, I_c, and $B_{c\perp}$. The right side y-axis of Figure. 4c shows the variation of the superconducting coherence length (ξ_{GL}) with D. At a given D, the Ginzburg Landau coherence length (ξ_{GL}) is extracted from the inferred zero temperature limit of the critical magnetic field, $B^0_{c\perp}$(see SI- 8 (IV) for details). Figure. 4d shows the effect on the SC phase of a parallel magnetic field, $B_{\parallel}$, and T at $D = 0.00$ V/nm (top panel) and $D = 0.60$ V/nm (bottom panel). The temperature dependence of $B_{c\parallel}$ (red dots in Figure. 4d) is fitted to the phenomenological relation: $T/T^0_c = 1 - (B_{c\parallel}/B^0_{c\parallel})^2$, where T^0_c is the superconducting critical temperature at zero B, and the fitting gives the critical parallel magnetic field in the zero temperature limit,

$B^0_{c\|}$, which matches well with the Pauli limit, B_P,[6,8,33] (see SI- 8 (V) for details) at $D = 0.00$ and 0.60 V/nm. Note that the asymmetry in SC metrics with positive and negative D seen in our experiment in Figure. 4 could be related to the asymmetry in the dielectric environment of the top and bottom layer graphene (different thicknesses of the top and bottom hBN, metallic top gate versus SiO_2/Si back gate, and discussed in detail in SI- 2 and SI- 3 (I)), and has been reported for alternatingly twisted trilayer graphene.[8,9]

Hall density and isospin symmetry breaking with D

So far, we have discussed how the SC is tuned with D; however, to see its connection with the characteristics of the band structure, in this section, we present the Fermiology measurements like the Hall density (n_H). The single particle low-energy band of tBLG has four flavors, corresponding to degenerate two valleys and two spins, as schematically shown in Figure. 5a. The combined spin and valley degrees of freedom are known as isospin symmetry. In MAtBLG, the isospin symmetries are spontaneously broken due to electron-electron interactions around the integer fillings, leading to isospin-polarized states. The breaking of isospin symmetry in twisted bilayer graphene is known as the 'cascaded' transitions, or 'reset,' or 'Dirac revival'.[8,35,36,49] The dependence of Hall density, n_H, with filling, ν, provides insight into whether the isospin symmetry is broken or not. Further, n_H can differentiate various phenomena; for instance, a gap opening or the presence of a vHs would cause the n_H to change sign, whereas, for isospin symmetry breaking, n_H will reduce and approach zero in a fully polarized case without changing sign. As the carrier density increases further, the n_H rises again, reflecting the number of remaining degeneracies. The details are described in SI-10 and schematically shown in SI-Fig. 16. Figure. 5d shows the variation

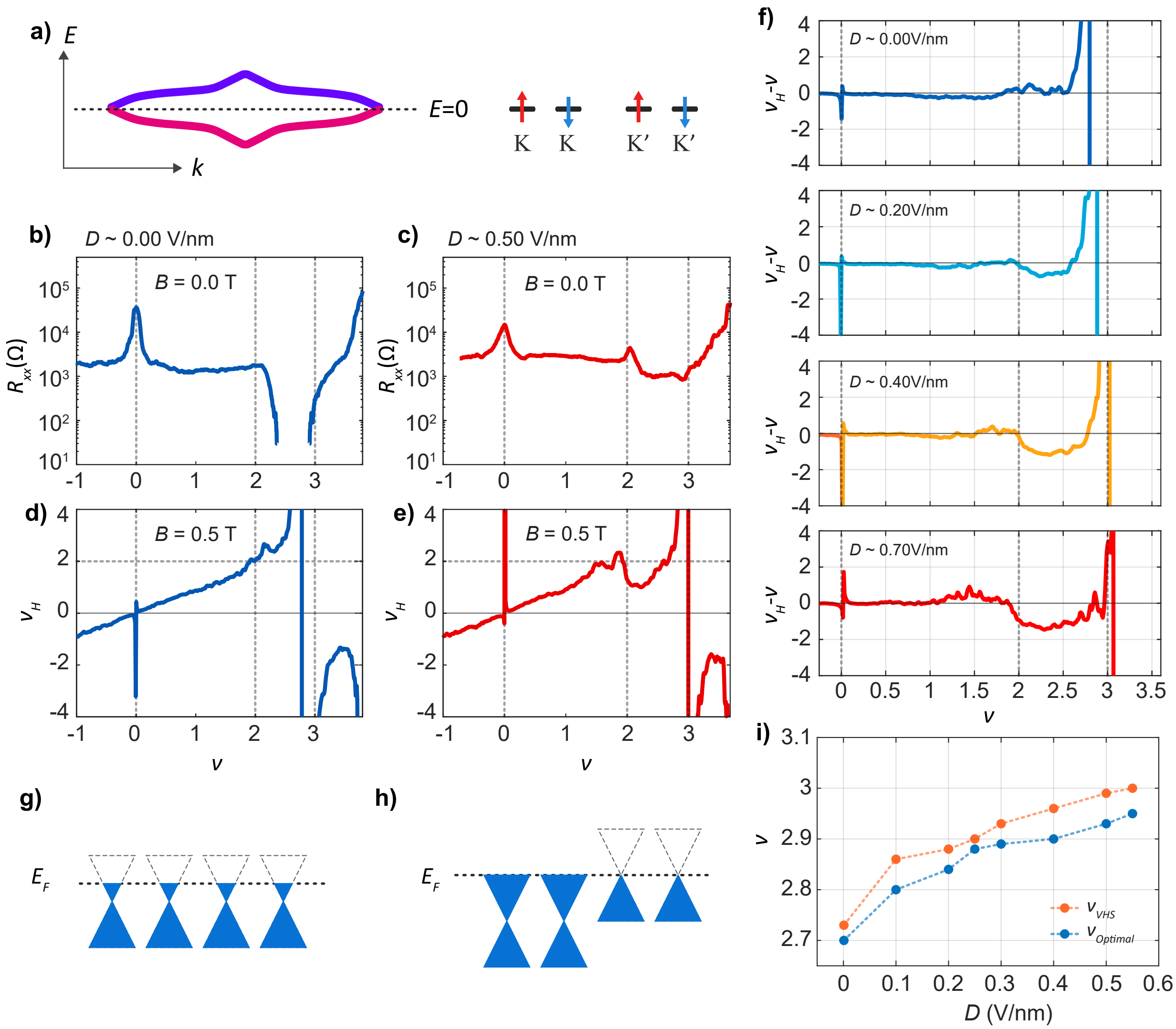

Figure. 5: Hall density and isospin symmetry breaking with D. a) Schematic representation of isospin unpolarized single particle low energy degenerate bands in tBLG. **b), c)** Longitudinal resistance, R_{xx} vs. the filling factor, ν, for displacement field, $D = 0.00$ V/nm and 0.50 V/nm respectively. **d), e)** Normalized Hall density ν_H vs. ν for the same D values as in **(b), (c). f)** $\nu_H - \nu$ vs. ν plots for several D. **g)** Schematic representation of unpolarized isospin flavors at zero D when all the Dirac-like bands are equally populated with degeneracy $g_d = 4$. **h)** Schematic representation for polarized isospin flavors with degeneracy $g_d = 2$. **i)** Filling factors of the optimal doping point of the superconducting phase, $\nu_{optimal}$ and the van Hove singularity (vHs) position, ν_{vHs} with D. Both $\nu_{optimal}$ and ν_{vHs} track each other and increase with increasing D.

of the measured Hall filling (normalized Hall density), ν_H ($\equiv 4n_H/n_s$) (see SI- 9 (II) for details), with the moiré filling factor, ν, at $D = 0.00$ V/nm on the electron-doped side at $B_\perp = 0.5$ T (anti-symmetrized by measuring at $B_\perp = \pm 0.5$ T, see SI- 9 (I) for details). At $B_\perp = 0.5$ T, the SC is killed, and it can be seen from Figure. 5d that ν_H increases with a linear slope until $\nu \sim +2$, and beyond that, ν_H increases rapidly and diverges (with value $> \pm 200$, see SI-Fig. 15a) on either side of $\nu \sim +2.7$, where it changes sign. This is a distinct clear signature of (the Fermi level crossing) a vHs.[9] It can be seen from the R_{xx} versus ν plot in Figure. 5b ($B_\perp = 0$ T) that the SC phase arises around the vHs, and the linear slope (unity) in the Hall filling (versus filling) measurement confirms that all the four flavours are equally populated with the charge carriers as shown schematically in Figure. 5g, implying that the SC arises from an isospin-unpolarized band. A similar result for twisted double bilayer graphene stabilized by WSe_2[6] has recently been reported, where the superconductivity emerges from unpolarized states near the van Hove singularities (vHs). Figure.s 5c,e show similar plots for $D = 0.50$ V/nm, in which case, initially, the ν_H increases with slope one; however, before reaching the vHs at $\nu \sim +3.0$, there is a suppression of ν_H around $\nu \sim +2$, where a resistance peak (R_{xx}) concomitantly emerges as shown in Figure. 5c, with no SC. The 2−d colormap of ν_H with ν and D is shown in SI-Fig. 17a. To understand the suppression in Hall filling with ν, in Figure. 5f, we plot $\nu_H - \nu$ versus ν, which remains close to zero at $D = 0.00$ V/nm, reconfirming the degeneracy of $g_d = 4$ of the occupied bands. As can be seen from the figure, with increasing D the values of $\nu_H - \nu$ deviate from zero and become negative between $\nu \sim +2$ and vHs, and their values head towards ~ -2, attaining the value of ~ -1.6 at $D \sim 0.70$ V/nm, which indicates broken isospin symmetry with $g_d \sim 2$ as schematically shown in Figure. 5h and SI-Fig. 16. Although, $\nu_H - \nu$ approaching

-2 indicates isospin symmetry breaking with a degeneracy of 2, and is a well-established method used in earlier reports;[6,8,9,18,50] a definitive proof would have been the observation of anomalous Hall effect (AHE) due to valley polarization or anomaly in R_{xx} response with $B_{\parallel}$ due to spin-polarizarion.[6] As shown in SI-13 and SI-14, neither AHE with $B_{\perp}$ nor anomaly in R_{xx} with $B_{\parallel}$ is observed, and this aligns with the prediction[51] that valley polarization or spin polarization at half filling is unlikely due to the inter-valley Hund's coupling. Further studies, such as local compressibility[35] or STM measurements,[36] are required to confirm the conclusive evidence of isospin symmetry breaking at the half-filling.

Discussion

To summarize the above section, for our device, SC arises around the vHs from an unpolarized band but becomes weaker with broken isospin symmetry (or cascaded transition/Dirac revival[35,36]) at $\nu \sim +2$, which is responsible for the appearance of the peak in R_{xx}. Though we do not see any signatures of an insulating behavior of the peak emerging with increasing $|D|$ at $\nu \sim +2$, these two competing phases, SC and the phase with isospin polarization, are stabilized respectively for small and large values of the displacement field. Though with increasing D, the SC phase gets suppressed, the intimate connection between the diverging density of states (vHs) and SC can be seen in Figure. 5i, where the filling values corresponding to the vHs (ν_{vHs}) and optimal doping for the SC ($\nu_{optimal}$) are plotted versus D and show a close correspondence. In our theory, using a tight-binding model (see SI- 15), we capture the shift of the vHs with increasing D as shown in SI-Fig. 22. Although the calculated position of fillings corresponding to the vHs do not precisely match experimental observations, the theory captures the essential features qualitatively. The effect of the shift of the vHs to higher Fermi level, μ, with an increasing electric field, E, and broadening of the density of states (DOS) around it are calculated in ref[52] (Fig. S4a) using the continuum model[37,53,54] for a MAtBLG ($\theta = 1.1^0$). Broadening of the low energy bandwidth and shift of the vHs with the applied displacement field, D, in experiments, has also been reported in other twisted platforms such as in twisted bilayer WSe_2.[55] We want to mention here that there are several other systems, such as rhombohedral trilayer graphene,[45] alternatingly twisted trilayer[8,9] and multilayer graphene,[10,11] in which the SC phase emerges directly from a phase where only two out of the four isospin components are occupied. In comparison, in twisted bilayer graphene, there have been contrasting results between MAtBLG and detuned[18] or screened tBLG.[17,19] For instance, in screened tBLG devices, no signature of symmetry breaking is observed, while in unscreened devices, symmetry breaking is present.[17,18] Regardless of whether symmetry breaking occurs or not, SC is observed in both cases. However, since these experiments are conducted on different devices with varying hBN thickness, it is not possible to directly compare the strength of the SC. Our results in a near MAtBLG device demonstrate that the isospin symmetry can be tuned by applying a displacement field, allowing us to study its impact on SC and establish that SC and isospin symmetry breaking compete with each other. Our observation aligns with recent theoretical findings reported on MAtBLG in Figure 2, and Fig. S4a of,[52] which also show that the SC becomes weaker in the isospin symmetry-broken state. It was noted[52] that an external electric field has a cumulative effect of reduction and smearing of the density of states (DOS) peaks, i.e., van Hove singularity (vHs), and hence reduces the critical temperature of the SC phase. It was also noted[52] that the instability of the Fermi-surface could be responsible for the isospin-symmetry breaking and lead to suppression of the SC phase. Similar physics is expected around the magic-angle; however, for detuned (away from the magic-angle) tBLG, further experimental and theoretical studies are required to find the role of displacement field on SC.

One could, in principle, argue that the modification with D of the SC phase could be due to the formation of superconducting percolation networks [12] arising from the possible presence of disorders. Here we would like to point out that we see (in Figure. 5e) a reduction of Hall filling, ν_H, at $\nu \sim +2$ with increasing D measured at $B_\perp = 0.5$ T ($B_{c\perp} \approx 60 - 70$ mT at $D = 0.00$ V/nm) where no superconductivity survives for any magnitude of $|D|$, leading to an isospin polarization with reduced degeneracy. The gradual increase of R_{xx} to a peak (in Figure. 5c) and simultaneous reduction of the ν_H near $\nu \approx +2$ with D, the synergy of both these phenomena can only be understood through the underlying modification of the low energy band structure of below magic-angle tBLG and cannot be reconciled with a picture of the percolating network of SC and normal state puddles. Moreover, the presence of a disorder-induced percolation network is expected to show the Fraunhofer pattern, which is not seen in our experiment for the strongest superconducting dome around $\nu \sim +2.7$ at $D = 0.00$ V/nm (Figure. 2d - left panel). The Fraunhofer pattern only arises after weakening the superconductivity at higher D as shown for $\nu \sim +2.3$ at $D = 0.53$ V/nm (Figure. 2d - right panel). Furthermore, the different thermal cycles (SI-Fig. 5) produce the same results in weakening the SC and the reduction in ν_H at $\nu \sim +2$ with increasing D, even though the disorder configurations are expected to be different in different thermal cycles. Further, the possible effect of contacts in our measured R_{xx} is discussed in SI- 3 (II) and ruled out its role in weakening SC. These observations indicate that the formation of superconducting percolation networks [12] arising from the possible presence of disorders or any other extrinsic origins are not responsible for the observed phenomena, rather our data suggest an intrinsic effect of the low energy band structure modification with electric field as seen in our theoretical calculations and consistent with ref.[52]

Conclusions

In summary, our findings emphasize the influence of band structure tuning through an external electric field on the emergence of superconductivity and other orders in near magic-angle twisted bilayer graphene. Our results shine a light on the close connection between the divergent density of states in the electronic structures (*i.e.*, vHs) and the presence of superconductivity in tBLG near magic-angle. Furthermore, we observe that superconductivity diminishes with alterations to the electronic structure when isospin gets polarized. Our results are consistent with the recent theoretical study showing the suppression of SC with electric field in tBLG, and highlight how the origin of SC in tBLG is special compared to other twisted and untwisted graphene-based heterostructures.[52]

Methods

Experimental: Device fabrication and measurement scheme:

The device consists of hBN-encapsulated twisted bilayer graphene (tBLG) on a SiO_2/Si substrate. The typical length and width of the devices are 6 μm and 2 μm, respectively. The usual 'tear and stack' technique[1,3] with a modification is used to fabricate the device and is described in detail in the Supplementary Information (SI- 1). We measured low-temperature transport in a cryo-free dilution refrigerator at $\sim 20-25$ mK. Using a constant bias current of $I \leq 5$ nA, the four-probe longitudinal (V_{xx}) and transverse voltage (V_{xy}) were measured (Figure. 1e) using a lock-in amplifier at a low frequency (~ 13 Hz).

Theory:

A tBLG structure of twist angle $\theta = 0.95°$ was generated using the TWISTER code.[56] The atomic positions were then relaxed in LAMMPS[57] up to a force tolerance of 10^{-6} ev/Å. Classical force fields were used to model the interatomic interactions, with Tersoff[58] as the intra-layer potential and DRIP[59] as the inter-layer potential. The electronic band structures were computed using a tight binding model with the transfer integrals approximated using the Slater-Koster formalism.[60] The displacement fields were integrated into the calculations as on-site terms within each layer, enabling the assessment of their impact on the electronic properties of the system. Although the doping levels, at which the van Hove singularities (vHs) occurred in our calculations are lower than those observed experimentally, the qualitative behavior and the evolution of the vHs on the electron side with displacement field are consistent with the experimental findings. Further details are available in the Supplementary Information (SI- 15).

Associated Content

A pre-print version of this work is available at ref.[61]

Supporting Information

Supplementary Information is available free of charge at

Device fabrication, device optical image, device response, and twist angle determination; Controlling the number density, n, and the displacement field, D; $\nu - D$ phase diagram from R_{xx}; dV_{xx}/dI vs. I_{DC} and $B_{\perp}$ at the optimal doping and near the edge of SC dome; Fraunhofer pattern observed at large D: signature of phase coherence in the SC phase; Various possible origins of the absence of resistance peak at the half filling at $D = 0$ V/nm; Method of extraction of the superconducting critical temperature, T_c; Raw data related to superconductivity metrics; R_{xy} and Hall filling factor, ν_H; Isospin symmetry and Hall density; $\nu - D$ phase diagram of normalized Hall density (Hall filling), ν_H; Differential resistance vs. ν at different D; Absence of Anomalous Hall Effect (AHE); R_{xx} in $B_{\parallel}$, and Theoretical calculations (PDF)

Data availability

All the relevant non-analytical line-plot data generated or measured during this study are included in this published article (and its Supplementary Information files). Additional information related to this work is available from the corresponding author upon reasonable request.

Code availability

The code that supports the findings of this study is available from the corresponding author upon reasonable request.

Author contributions

R.D. contributed to device fabrication. R.D. and A.G. contributed to data acquisition and analysis. A.G. also contributed to developing measuring codes. S.M., H.R.K., S.B., and M.J. contributed to the development of the theory. K.W. and T.T. synthesized the hBN single crystals. A.D. contributed to conceiving the idea and designing the experiment, data interpretation, and analysis. All the authors contributed to the data interpretation and writing of the manuscript.

Notes

The authors declare no competing financial interest.

Acknowledgements

A.D. thanks Ashvin Vishwanath, Mohit Randeria, and Nandini Trivedi for the useful discussions. R.D. is grateful to Manabendra Kuiri, Arup Kumar Paul, Ravi Kumar, Saurabh Kumar Srivastav, Souvik Chakraborty, and Ujjal Roy for numerous discussions on the fabrication of twisted heterostructures. R.D. and A.G. thank Ujjal Roy, Dr. Saurabh Kumar Srivastav, Dr. Ravi Kumar, and Souvik Chakraborty for their assistance while doing measurements in the He^3 cryo-stat (Oxford Heliox) and cryo-free dilution refrigerator (Oxford

Triton and Oxford Proteox). H.R.K. and M.J. gratefully acknowledge the National Supercomputing Mission of the Department of Science and Technology, India, and the Science and Engineering Research Board of the Department of Science and Technology, India, for financial support under Grants No. DST/NSM/R&D HPC Applications/2021/23 and No. SB/DF/005/2017, respectively. H.R.K. also acknowledges support from the Indian National Science Academy under its grant no. INSA/SP/SS/2023/. A.D. thanks the Department of Science and Technology Nano Mission (DST/NM/TUE/QM-5/2019(C)/1) and Science and Engineering Research Board (SERB), India, for financial support (SP/SERB-22-0387) and acknowledges funding through the Intensification of Research in High Priority Areas programme of the Science and Engineering Research Board (Grant No. IPA/2020/000034). A.D. also thanks CEFIPRA project SP/IFCP-22-0005. Growing the hBN crystals received support from the Japan Society for the Promotion of Science (KAKENHI grant nos. 19H05790, 20H00354 and 21H05233) to K.W. and T.T.

References

(1) Cao, Y.; Fatemi, V.; Fang, S.; Watanabe, K.; Taniguchi, T.; Kaxiras, E.; Jarillo-Herrero, P. Unconventional Superconductivity in Magic-Angle Graphene Superlattices. *Nature* **2018**, *556*, 43–50.

(2) Lu, X.; Stepanov, P.; Yang, W.; Xie, M.; Aamir, M. A.; Das, I.; Urgell, C.; Watanabe, K.; Taniguchi, T.; Zhang, G.; others Superconductors, Orbital Magnets and Correlated States in Magic-Angle Bilayer Graphene. *Nature* **2019**, *574*, 653–657.

(3) Cao, Y.; Fatemi, V.; Demir, A.; Fang, S.; Tomarken, S. L.; Luo, J. Y.; Sanchez-Yamagishi, J. D.; Watanabe, K.; Taniguchi, T.; Kaxiras, E.; others Correlated Insulator Behaviour at Half-Filling in Magic-Angle Graphene Superlattices. *Nature* **2018**, *556*, 80–84.

(4) Liu, X.; Hao, Z.; Khalaf, E.; Lee, J. Y.; Ronen, Y.; Yoo, H.; Haei Najafabadi, D.; Watanabe, K.; Taniguchi, T.; Vishwanath, A.; others Tunable Spin-Polarized Correlated States in Twisted Double Bilayer Graphene. *Nature* **2020**, *583*, 221–225.

(5) Cao, Y.; Rodan-Legrain, D.; Rubies-Bigorda, O.; Park, J. M.; Watanabe, K.; Taniguchi, T.; Jarillo-Herrero, P. Tunable Correlated States and Spin-Polarized Phases in Twisted Bilayer–Bilayer Graphene. *Nature* **2020**, *583*, 215–220.

(6) Su, R.; Kuiri, M.; Watanabe, K.; Taniguchi, T.; Folk, J. Superconductivity in Twisted Double Bilayer Graphene Stabilized by WSe2. *Nature Materials* **2023**, *22*, 1332–1337.

(7) Kuiri, M.; Coleman, C.; Gao, Z.; Vishnuradhan, A.; Watanabe, K.; Taniguchi, T.; Zhu, J.; MacDonald, A. H.; Folk, J. Spontaneous Time-Reversal Symmetry Breaking in Twisted Double Bilayer Graphene. *Nature Communications* **2022**, *13*, 6468.

(8) Park, J. M.; Cao, Y.; Watanabe, K.; Taniguchi, T.; Jarillo-Herrero, P. Tunable Strongly

Coupled Superconductivity in Magic-Angle Twisted Trilayer Graphene. *Nature* **2021**, *590*, 249–255.

(9) Hao, Z.; Zimmerman, A.; Ledwith, P.; Khalaf, E.; Najafabadi, D. H.; Watanabe, K.; Taniguchi, T.; Vishwanath, A.; Kim, P. Electric Field–Tunable Superconductivity in Alternating-Twist Magic-Angle Trilayer Graphene. *Science* **2021**, *371*, 1133–1138.

(10) Park, J. M.; Cao, Y.; Xia, L.-Q.; Sun, S.; Watanabe, K.; Taniguchi, T.; Jarillo-Herrero, P. Robust Superconductivity in Magic-Angle Multilayer Graphene Family. *Nature Materials* **2022**, *21*, 877–883.

(11) Zhang, Y.; Polski, R.; Lewandowski, C.; Thomson, A.; Peng, Y.; Choi, Y.; Kim, H.; Watanabe, K.; Taniguchi, T.; Alicea, J.; others Promotion of Superconductivity in Magic-Angle Graphene Multilayers. *Science* **2022**, *377*, 1538–1543.

(12) Yankowitz, M.; Chen, S.; Polshyn, H.; Zhang, Y.; Watanabe, K.; Taniguchi, T.; Graf, D.; Young, A. F.; Dean, C. R. Tuning Superconductivity in Twisted Bilayer Graphene. *Science* **2019**, *363*, 1059–1064.

(13) Cao, Y.; Rodan-Legrain, D.; Park, J. M.; Yuan, N. F. Q.; Watanabe, K.; Taniguchi, T.; Fernandes, R. M.; Fu, L.; Jarillo-Herrero, P. Nematicity and Competing Orders in Superconducting Magic-Angle Graphene. *Science* **2021**, *372*, 264–271.

(14) Paul, A. K.; Ghosh, A.; Chakraborty, S.; Roy, U.; Dutta, R.; Watanabe, K.; Taniguchi, T.; Panda, A.; Agarwala, A.; Mukerjee, S.; others Interaction-Driven Giant Thermopower in Magic-Angle Twisted Bilayer Graphene. *Nature Physics* **2022**, 1–8.

(15) Codecido, E.; Wang, Q.; Koester, R.; Che, S.; Tian, H.; Lv, R.; Tran, S.; Watanabe, K.; Taniguchi, T.; Zhang, F.; others Correlated Insulating and Superconducting States in Twisted Bilayer Graphene Below the Magic Angle. *Science Advances* **2019**, *5*, eaaw9770.

(16) Arora, H. S.; Polski, R.; Zhang, Y.; Thomson, A.; Choi, Y.; Kim, H.; Lin, Z.; Wilson, I. Z.; Xu, X.; Chu, J.-H.; others Superconductivity in Metallic Twisted Bilayer Graphene Stabilized by WSe2. *Nature* **2020**, *583*, 379–384.

(17) Stepanov, P.; Das, I.; Lu, X.; Fahimniya, A.; Watanabe, K.; Taniguchi, T.; Koppens, F. H.; Lischner, J.; Levitov, L.; Efetov, D. K. Untying the Insulating and Superconducting Orders in Magic-Angle Graphene. *Nature* **2020**, *583*, 375–378.

(18) Saito, Y.; Ge, J.; Watanabe, K.; Taniguchi, T.; Young, A. F. Independent Superconductors and Correlated Insulators in Twisted Bilayer Graphene. *Nature Physics* **2020**, *16*, 926–930.

(19) Liu, X.; Wang, Z.; Watanabe, K.; Taniguchi, T.; Vafek, O.; Li, J. Tuning Electron Correlation in Magic-Angle Twisted Bilayer Graphene Using Coulomb Screening. *Science* **2021**, *371*, 1261–1265.

(20) Tian, H.; Gao, X.; Zhang, Y.; Che, S.; Xu, T.; Cheung, P.; Watanabe, K.; Taniguchi, T.; Randeria, M.; Zhang, F.; others Evidence for Dirac Flat Band Superconductivity Enabled by Quantum Geometry. *Nature* **2023**, *614*, 440–444.

(21) Po, H. C.; Zou, L.; Vishwanath, A.; Senthil, T. Origin of Mott Insulating Behavior and Superconductivity in Twisted Bilayer Graphene. *Phys. Rev. X* **2018**, *8*, 031089.

(22) Sharpe, A. L.; Fox, E. J.; Barnard, A. W.; Finney, J.; Watanabe, K.; Taniguchi, T.; Kastner, M.; Goldhaber-Gordon, D. Emergent Ferromagnetism Near Three-Quarters Filling in Twisted Bilayer Graphene. *Science* **2019**, *365*, 605–608.

(23) Tseng, C.-C.; Ma, X.; Liu, Z.; Watanabe, K.; Taniguchi, T.; Chu, J.-H.; Yankowitz, M. Anomalous Hall Effect at Half Filling in Twisted Bilayer Graphene. *Nature Physics* **2022**, *18*, 1038–1042.

(24) Serlin, M.; Tschirhart, C. L.; Polshyn, H.; Zhang, Y.; Zhu, J.; Watanabe, K.; Taniguchi, T.; Balents, L.; Young, A. F. Intrinsic Quantized Anomalous Hall Effect in a Moiré Heterostructure. *Science* **2020**, *367*, 900–903.

(25) Saito, Y.; Ge, J.; Rademaker, L.; Watanabe, K.; Taniguchi, T.; Abanin, D. A.; Young, A. F. Hofstadter Subband Ferromagnetism and Symmetry-Broken Chern Insulators in Twisted Bilayer Graphene. *Nature Physics* **2021**, *17*, 478–481.

(26) Wu, S.; Zhang, Z.; Watanabe, K.; Taniguchi, T.; Andrei, E. Y. Chern Insulators, van Hove singularities and Topological Flat Bands in Magic-Angle Twisted Bilayer Graphene. *Nature Materials* **2021**, *20*, 488–494.

(27) Das, I.; Lu, X.; Herzog-Arbeitman, J.; Song, Z.-D.; Watanabe, K.; Taniguchi, T.; Bernevig, B. A.; Efetov, D. K. Symmetry-Broken Chern Insulators and Rashba-Like Landau-Level Crossings in Magic-Angle Bilayer Graphene. *Nature Physics* **2021**, *17*, 710–714.

(28) Chen, G.; Sharpe, A. L.; Fox, E. J.; Zhang, Y.-H.; Wang, S.; Jiang, L.; Lyu, B.; Li, H.; Watanabe, K.; Taniguchi, T.; others Tunable Correlated Chern Insulator and Ferromagnetism in a Moiré Superlattice. *Nature* **2020**, *579*, 56–61.

(29) Pierce, A. T.; Xie, Y.; Park, J. M.; Khalaf, E.; Lee, S. H.; Cao, Y.; Parker, D. E.; Forrester, P. R.; Chen, S.; Watanabe, K.; others Unconventional Sequence of Correlated Chern Insulators in Magic-Angle Twisted Bilayer Graphene. *Nature Physics* **2021**, *17*, 1210–1215.

(30) Cao, Y.; Chowdhury, D.; Rodan-Legrain, D.; Rubies-Bigorda, O.; Watanabe, K.; Taniguchi, T.; Senthil, T.; Jarillo-Herrero, P. Strange Metal in Magic-Angle Graphene with Near Planckian Dissipation. *Physical review letters* **2020**, *124*, 076801.

(31) Ghawri, B.; Mahapatra, P. S.; Garg, M.; Mandal, S.; Bhowmik, S.; Jayaraman, A.; Soni, R.; Watanabe, K.; Taniguchi, T.; Krishnamurthy, H.; others Breakdown of

Semiclassical Description of Thermoelectricity in Near-Magic Angle Twisted Bilayer Graphene. *Nature Communications* **2022**, *13*, 1522.

(32) Ghosh, A.; Chakraborty, S.; Dutta, R.; Agarwala, A.; Watanabe, K.; Taniguchi, T.; Banerjee, S.; Trivedi, N.; Mukerjee, S.; Das, A. Evidence of Enhanced Thermopower from Emergent Local Moments in Flatbands of Magic-Angle Twisted Bilayer Graphene. *arXiv preprint arXiv:2403.08686* **2024**,

(33) Cao, Y.; Park, J. M.; Watanabe, K.; Taniguchi, T.; Jarillo-Herrero, P. Pauli-Limit Violation and Re-Entrant Superconductivity in Moiré Graphene. *Nature* **2021**, *595*, 526–531.

(34) Lin, J.-X.; Zhang, Y.-H.; Morissette, E.; Wang, Z.; Liu, S.; Rhodes, D.; Watanabe, K.; Taniguchi, T.; Hone, J.; Li, J. Spin-Orbit–Driven Ferromagnetism at Half Moiré Filling in Magic-Mngle Twisted Bilayer Graphene. *Science* **2022**, *375*, 437–441.

(35) Zondiner, U.; Rozen, A.; Rodan-Legrain, D.; Cao, Y.; Queiroz, R.; Taniguchi, T.; Watanabe, K.; Oreg, Y.; von Oppen, F.; Stern, A.; others Cascade of Phase Transitions and Dirac Revivals in Magic-Angle Graphene. *Nature* **2020**, *582*, 203–208.

(36) Wong, D.; Nuckolls, K. P.; Oh, M.; Lian, B.; Xie, Y.; Jeon, S.; Watanabe, K.; Taniguchi, T.; Bernevig, B. A.; Yazdani, A. Cascade of Electronic Transitions in Magic-Angle Twisted Bilayer Graphene. *Nature* **2020**, *582*, 198–202.

(37) Bistritzer, R.; MacDonald, A. H. Moiré Bands in Twisted Double-Layer Graphene. *Proceedings of the National Academy of Sciences* **2011**, *108*, 12233–12237.

(38) Xu, Z. A.; Ong, N. P.; Wang, Y.; Kakeshita, T.; Uchida, S. Vortex-Like Excitations and the Onset of Superconducting Phase Fluctuation in Underdoped La2-xSrxCuO4. *Nature* **2000**, *406*, 486–488.

(39) Lian, B.; Wang, Z.; Bernevig, B. A. Twisted Bilayer Graphene: A Phonon-Driven Superconductor. *Physical review letters* **2019**, *122*, 257002.

(40) Cea, T.; Guinea, F. Coulomb Interaction, Phonons, and Superconductivity in Twisted Bilayer Graphene. *Proceedings of the National Academy of Sciences* **2021**, *118*, e2107874118.

(41) Shavit, G.; Berg, E.; Stern, A.; Oreg, Y. Theory of Correlated Insulators and Superconductivity in Twisted Bilayer Graphene. *Physical review letters* **2021**, *127*, 247703.

(42) Zhou, H.; Holleis, L.; Saito, Y.; Cohen, L.; Huynh, W.; Patterson, C. L.; Yang, F.; Taniguchi, T.; Watanabe, K.; Young, A. F. Isospin Magnetism and Spin-Polarized Superconductivity in Bernal Bilayer Graphene. *Science* **2022**, *375*, 774–778.

(43) Zhang, Y.; Polski, R.; Thomson, A.; Lantagne-Hurtubise, É.; Lewandowski, C.; Zhou, H.; Watanabe, K.; Taniguchi, T.; Alicea, J.; Nadj-Perge, S. Enhanced Superconductivity in Spin–Orbit Proximitized Bilayer Graphene. *Nature* **2023**, *613*, 268–273.

(44) Li, C.; Xu, F.; Li, B.; Li, J.; Li, G.; Watanabe, K.; Taniguchi, T.; Tong, B.; Shen, J.; Lu, L.; others Tunable Superconductivity in Electron-and Hole-Doped Bernal Bilayer Graphene. *Nature* **2024**, 1–7.

(45) Zhou, H.; Xie, T.; Taniguchi, T.; Watanabe, K.; Young, A. F. Superconductivity in Rhombohedral Trilayer Graphene. *Nature* **2021**, *598*, 434–438.

(46) Chen, G.; Sharpe, A. L.; Gallagher, P.; Rosen, I. T.; Fox, E. J.; Jiang, L.; Lyu, B.; Li, H.; Watanabe, K.; Taniguchi, T.; others Signatures of Tunable Superconductivity in a Trilayer Graphene Moiré Superlattice. *Nature* **2019**, *572*, 215–219.

(47) Ghosh, A.; Chakraborty, S.; Ghorai, U.; Paul, A. K.; Watanabe, K.; Taniguchi, T.; Sensarma, R.; Das, A. Evidence of Compensated Semimetal with Electronic Correlations

at Charge Neutrality of Twisted Double Bilayer Graphene. *Communications Physics* **2023**, *6*, 360.

(48) Zhou, Z.; Jiang, J.; Karnatak, P.; Wang, Z.; Wagner, G.; Watanabe, K.; Taniguchi, T.; Schönenberger, C.; Parameswaran, S.; Simon, S. H.; others Double-Dome Unconventional Superconductivity in Twisted Trilayer Graphene. *arXiv preprint arXiv:2404.09909* **2024**,

(49) Rozen, A.; Park, J. M.; Zondiner, U.; Cao, Y.; Rodan-Legrain, D.; Taniguchi, T.; Watanabe, K.; Oreg, Y.; Stern, A.; Berg, E.; others Entropic Evidence for a Pomeranchuk Effect in Magic-Angle Graphene. *Nature* **2021**, *592*, 214–219.

(50) Liu, X.; Zhang, N. J.; Watanabe, K.; Taniguchi, T.; Li, J. Isospin order in superconducting magic-angle twisted trilayer graphene. *Nature Physics* **2022**, *18*, 522–527.

(51) Bultinck, N.; Chatterjee, S.; Zaletel, M. P. Mechanism for Anomalous Hall Ferromagnetism in Twisted Bilayer Graphene. *Physical review letters* **2020**, *124*, 166601.

(52) Long, M.; Jimeno-Pozo, A.; Sainz-Cruz, H.; Pantaleón, P. A.; Guinea, F. Evolution of Superconductivity in Twisted Graphene Multilayers. *Proceedings of the National Academy of Sciences* **2024**, *121*, e2405259121.

(53) Lopes dos Santos, J.; Peres, N.; Castro Neto, A. Graphene Bilayer with a Twist: Electronic Structure. *Physical review letters* **2007**, *99*, 256802.

(54) Koshino, M.; Nam, N. N. Effective Continuum Model for Relaxed Twisted Bilayer Graphene and Moiré Electron-Phonon Interaction. *Physical Review B* **2020**, *101*, 195425.

(55) Wang, L.; Shih, E.-M.; Ghiotto, A.; Xian, L.; Rhodes, D. A.; Tan, C.; Claassen, M.; Kennes, D. M.; Bai, Y.; Kim, B.; others Correlated Electronic Phases in Twisted Bilayer Transition Metal Dichalcogenides. *Nature materials* **2020**, *19*, 861–866.

(56) Naik, S.; Naik, M. H.; Maity, I.; Jain, M. Twister: Construction and Structural Relaxation of Commensurate Moiré Superlattices. *Computer Physics Communications* **2022**, *271*, 108184.

(57) Thompson, A. P.; Aktulga, H. M.; Berger, R.; Bolintineanu, D. S.; Brown, W. M.; Crozier, P. S.; in't Veld, P. J.; Kohlmeyer, A.; Moore, S. G.; Nguyen, T. D.; others LAMMPS-a Flexible Simulation Tool for Particle-Based Materials Modeling at the Atomic, Meso, and Continuum Scales. *Computer Physics Communications* **2022**, *271*, 108171.

(58) Kınacı, A.; Haskins, J. B.; Sevik, C.; Çağın, T. Thermal Conductivity of BN-C Nanostructures. *Physical Review B* **2012**, *86*, 115410.

(59) Wen, M.; Carr, S.; Fang, S.; Kaxiras, E.; Tadmor, E. B. Dihedral-Angle-Corrected Registry-Dependent Interlayer Potential for Multilayer Graphene Structures. *Physical Review B* **2018**, *98*, 235404.

(60) Moon, P.; Koshino, M. Energy Spectrum and Quantum Hall Effect in Twisted Bilayer Graphene. *Physical Review B* **2012**, *85*, 195458.

(61) Dutta, R.; Ghosh, A.; Mandal, S.; Watanabe, K.; Taniguchi, T.; Krishnamurthy, H.; Banerjee, S.; Jain, M.; Das, A. Electric field tunable superconductivity with competing orders in near magic-angle twisted bilayer graphene. *arXiv preprint arXiv:2402.11649v2* **2024** https://arxiv.org/abs/2402.11649,

Table of Content Figure

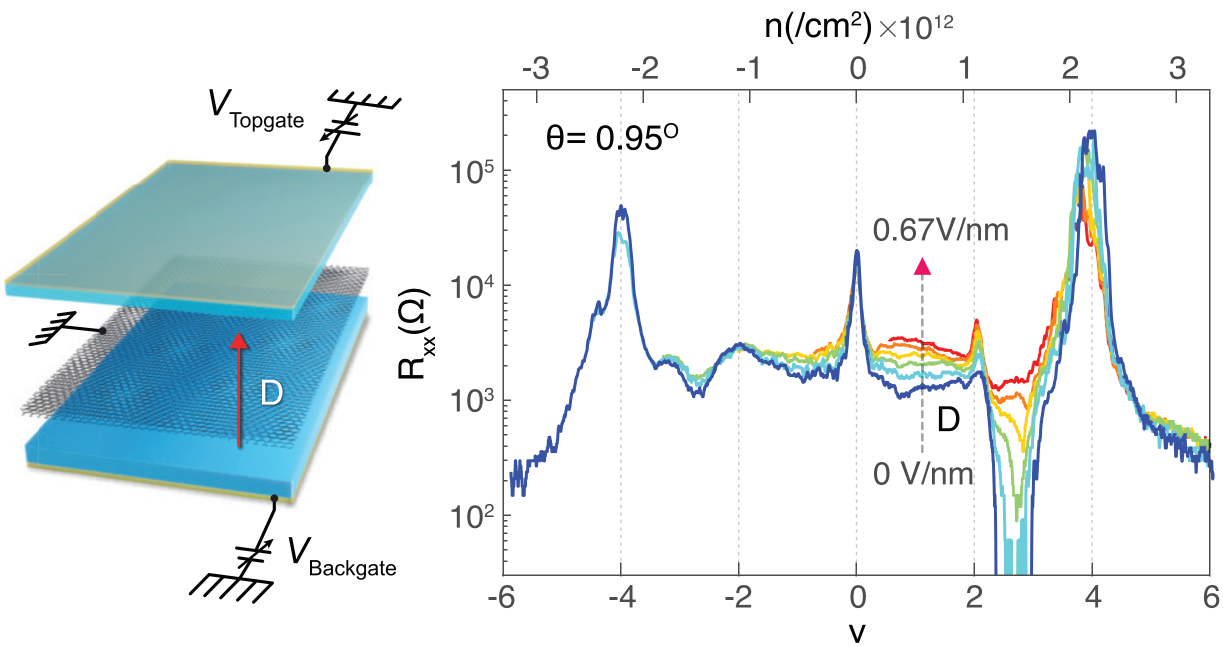

Figure. 6: For Table of Contents Only.